Two-Dimensional Penning Ionization Electron Spectroscopy of 2-Aminoethanol and Related Molecules by He*(2^3S) Atoms: Influence of Intramolecular Hydrogen Bonding on Collisional Ionization

Ryo Maruyama and Koichi Ohno*

Department of Chemistry, Graduate School of Science, Tohoku University, Aramaki, Aoba-ku, Sendai 980-8578, Japan

Received: December 22, 2003

Penning ionization of 2-aminoethanol (AE), ethylamine (EA), *N*-methyl-2-aminoethanol (MAE), and 2-methoxy-*N*-methylethylamine (MMA) upon collision with He*(2^3S) metastable atoms has been studied by two-dimensional electron-energy/collision-energy-resolved Penning ionization electron spectroscopy (2D-PIES) in connection with intramolecular hydrogen bonding of OH···N and NH···O types. In AE and MAE, OH···N type hydrogen bonds were found to be preferentially formed, whereas in MAE, observed data gave a confirmation of the NH···O type hydrogen bond. Effects of hydrogen bond formation were observed for ionization bands of nonbonding orbitals related to the hydrogen bond. Associated with hydrogen bond formation, the relative band intensity in PIES become considerably decreased, the slope of the collision energy dependence of partial ionization cross section become much less negative, and the peak energy shift becomes much less negative.

I. Introduction

To elucidate chemical reactions, it is important to investigate dynamics of particles on the anisotropic interaction potential energy surface. When a metastable rare gas atom A* collides with a reactant molecule M, provided that A* has an excitation energy larger than the lowest ionization potential (IP) of M, an ionization process known as Penning ionization can occur[1−3]

$$A^* + M \rightarrow M^+ + A + e^-$$

Kinetic-energy spectra of electrons (e^-) ejected in this collisional ionization process are called Penning ionization electron spectra (PIES).[4] The kinetic energy of the ejected electron (E_e) is equal to the difference between two potential energy functions, the incoming M + A* interaction potential V* and the outgoing A + M^+ interaction potential V^+. Both of these are functions of the internuclear distance R between the metastable atom and the molecule, and the kinetic energy E_e of Penning electron is determined by

$$E_e(R) = V^*(R) - V^+(R) = E(A^*) - IP + \Delta E(R)$$

where E(A*) is the excitation energy of the metastable atom A* and ΔE is the peak energy shift in PIES with respect to the peak positions observed in ultraviolet photoelectron spectra (UPS). ΔE is negative if the incoming interaction potential is attractive, and it becomes positive if the potential is repulsive.

On the other hand, branching ratios are different between PIES and UPS, depending on their ionization mechanisms. The Penning ionization process can be explained on the basis of the electron-exchange model requiring overlap between relevant orbitals.[7] Ohno et al.[8,9] proposed the exterior electron density (EED) model to this process in order to account for experimental branching ratios of Penning ionization. On the basis of this model, PIES provide us information on the electron distributions of molecular orbitals (MO) exposed outside the boundary surface (repulsive molecular surface) of collision. In Penning ionization, the most effective direction for the collisional ionization is different depending on the more or less localized electron distributions of the target MO. Therefore, the collision energy dependence of a partial ionization cross section, $\sigma_i(E_c)$ for the ith ionic state, enables us to investigate the anisotropic potential energy surface around the target molecule. If the ionization reaction occurs under a strong influence of attractive interactions, the ionization cross section should enhance at lower collision energies, because a slower A* atom can approach the reactive region effectively. On the other hand, if the ionization reaction occurs under a strong influence of repulsive interactions, the ionization cross section should increase at higher collision energy regions, because a faster A* atom can approach the reactive region at shorter distances.

An experimental technique[10] has been developed to obtain two-dimensional PIES (2D-PIES) in which ionization cross sections are as functions of both electron kinetic energy (E_e) and collision energy (E_c). Collision energy dependence of partial ionization cross sections (CEDPICS), which reflects anisotropic interactions between M and He*, has been observed for N_2 and some simple molecules,[11−13] organic molecules including heteroatoms,[14] benzene,[15,16] substituted benzenes,[17,18] and an organometallic compound.[19]

Conformational isomerism in 2-aminoethanol has been a subject of theoretical[20−26] and experimental[27−33] studies. In 2-aminoethanol, two types of intramolecular hydrogen bonding, OH···N and NH···O, should be considered. Microwave,[27−30] infrared,[31] and electron spectroscopic[32,33] studies as well as ab initio calculations[20−26] showed that the former type hydrogen bonding gives the most stable conformer in the gaseous phase.

* To whom correspondence should be addressed. Phone: +81-22-217-6576. Fax: +81-22-217-6580. E-mail: ohnok@qpcrkk.chem.tohoku.ac.jp.

10.1021/jp0379695 CCC: $27.50
Published on Web 04/16/2004

It is interesting to study effects of intramolecular hydrogen bonding on the interaction potentials around the molecule.

In this study, we have measured 2D-PIES of 2-aminoethanol (AE: $NH_2CH_2CH_2OH$), ethylamine (EA: $CH_3CH_2NH_2$), *N*-methyl-2-aminoethanol (MAE: $NH(CH_3)CH_2CH_2OH$), and 2-methoxy-*N*-methylethylamine (MMA: $NH(CH_3)CH_2CH_2OCH_3$). Collisional ionization dynamics as well as anisotropic interaction potentials around the target molecules, especially around N and O atoms, were investigated in connection with intramolecular hydrogen bonding.

II. Experimental Section

High-purity samples of AE, EA, MAE, and MMA were purchased from Tokyo KASEI KOGYO Co., Ltd. and further purified by several freeze−pump−thaw cycles. Details of experimental apparatus for He*(2^3S) Penning ionization electron spectroscopy has been reported.[11] The metastable He* beam was generated by a discharge nozzle source with a hollow cathode.[11,34] The He* beam contains He*(2^1S) with an excitation energy smaller than He*(2^3S). He*(2^1S) atoms are optically quenched by a water-cooled helium discharge lamp after passing through a skimmer. He^+ ions and Rydberg species were removed by an electric deflector. The He*(2^3S) metastable beam was introduced into the collision cell. For measurements of He I UPS, He I resonance photons (584 nm, 21.22 eV) were produced by a discharge in pure helium gas. Sample gas was introduced in the collision cell where Penning ionization or photoionization occurs. Produced electrons were measured by a hemispherical electrostatic deflection type analyzer using an electron collection angle 90° to the incident He* beam or the He I resonance light. The energy resolution of the electron energy analyzer was estimated to be 60 meV from the full width at the half-maximum (fwhm) of the $Ar^+(^2P_{3/2})$ peak in the He I UPS. The transmission efficiency curve of the electron analyzer was determined by comparing our UPS data with those by Gardner and Samson[35] and Kimura et al.[36] Under these conditions, PIES without velocity selection and UPS were measured.

For collision-energy-resolved measurements, the energy resolution of the analyzer was lowered to 250 meV in order to obtain higher count rates. Two-dimensional signals $I_e(E_e, t)$ were obtained as a function of electron kinetic energy E_e and time t by the two-dimensional technique[13] and a cross-correlation time-of-flight (CC-TOF) method with a pseudorandom chopper.[37] The CC-TOF signals of $I_e(E_e, t)$ by the pseudorandom chopper were converted to the normal TOF signals $I_e(E_e, t_{TOF})$ by the Hadamard transformation. The two-dimensional signals $I_e(E_e, t_{TOF})$ were transformed to $I_e(E_e, v_{He^*})$ as a function of the velocity of He* and then to two-dimensional Penning ionization cross sections $\sigma(E_e, v_r)$ by the following equations:

$$\sigma(E_e, v_r) = c\{I_e(E_e, v_{He^*})/I_{He^*}(v_{He^*})\}(v_{He^*}/v_r)$$

$$v_r = [v_{He^*} + 3kT/M]^{1/2}$$

where c is a constant, v_r is the relative velocity averaged over the velocity of the target molecule, k is the Boltzmann constant, and T and M are the gas temperature and the mass of the target molecule, respectively. Finally, $\sigma(E_e, v_r)$ is converted to $\sigma(E_e, E_c)$ as functions of the electron energy E_e and the collision energy E_c by the relation

$$E_c = \mu v_r^2/2$$

where μ is the reduced mass of the system. Thus, 2D-PIES were obtained as $\sigma(E_e, E_c)$. CEDPICS were then obtained from an appropriate E_e range of $\sigma(E_e, E_c)$ within 250 meV with a caution to avoid contributions from neighboring bands.

III. Calculations

Among many possible conformations, only those of amino and methyl substituted amino groups were considered in the present calculations. The geometry of the AE was taken from microwave spectroscopic study.[27,28] Starting from initial structures deduced from microwave data,[27,28,38] geometry optimization calculations were made for MAE and MMA by the DFT method with Becke's three-parameter exchange with Lee, Young, and Parr correlation function (B3LYP)[39] with the 6-31+G* basis set. Interaction potential energies between He*(2^3S) and molecule M in various directions and angles were calculated on the basis of the well-known resemblance between He*(2^3S) and Li(2^2S);[41] the shape of the velocity dependence of the total scattering cross section of He*(2^3S) by He, Ar, and Kr is very similar to that of Li, and the location of the interaction potential well and its depth are similar for He*(2^3S) and Li with various targets.[42−45] Because of these findings and difficulties associated with calculations for excited states, the Li atom was used in this study in place of the He*(2^3S) atom. Thus, interaction potentials M + Li(2^2S) were calculated as functions of the distance between the Li atom and the N atom with keeping the molecular geometries fixed, provided that the geometry change by the approach of a metastable atom is negligible in the collision ionization process. Calculations of the interaction potentials were performed in the level of the second-order Møller−Plesset perturbation theory (MP2) with the 6-311++G** basis set. To obtain electron density contour maps of MO, ab initio self-consistent field calculations were performed with the 6-31+G* basis set. In electron density maps, thick solid curves indicate the repulsive molecular surface approximated by van der Waals radii[40] (r_C = 1.7 Å, r_N = 1.5 Å, r_O = 1.4 Å, r_H = 1.2 Å). All quantum chemical calculations were carried out with the Gaussian 98 program.[46]

IV. Results

Figures 1−4 show the He I UPS and He*(2^3S) PIES of AE, EA, MAE, and MMA, respectively. The electron energy scales for PIES are shifted by 1.40 eV relative to those for UPS due to the excitation energy difference of He I photons (21.22 eV) and He*(2^3S) (19.82 eV). Band labels in UPS are based on orbital characters and symmetries. Figures 5−8 show the log σ vs log E_c plots of CEDPICS in a collision energy range of 80−290 meV for AE, EA, MAE, and MMA, respectively. The plots of CEDPICS for various ionic states were shown in the arbitrary unit in order to avoid superposition of many curves. Electron density maps and schematic representation of the molecular orbitals are also shown in the figures, because important directions of He*(2^3S) atoms causing ionization are governed by regions of high electron densities outside the molecular surface. The maps are shown on the molecular NCC plane. In the schematic representation of molecular orbitals, circles and ellipses were used, as in a previous study.[47] In-plane p-type orbitals, the out-of-plane component of p orbitals, and valence s orbitals ware shown by couples of ellipses, a dashed circle, and solid circles, respectively.

Tables 1−4 list observed IP determined from the He I UPS (IP_{obsd}), calculated IP (IP_{calcd}), and assignments of observed bands for AE, EA, MAE, and MMA, respectively. Calculated IP of MAE in Table 3 were those for a structure with an

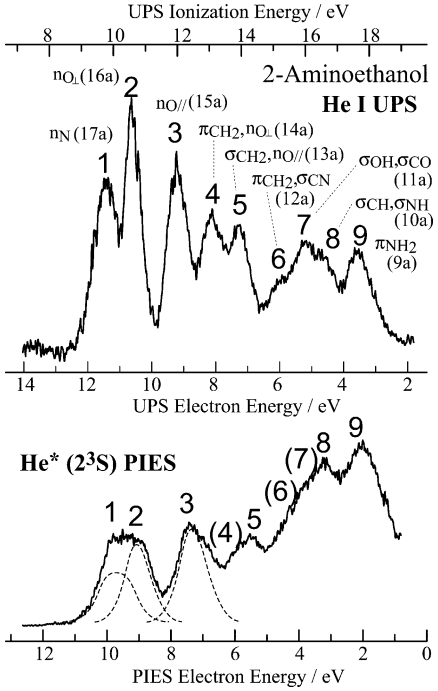

Figure 1. He I UPS and He*(2^3S) PIES of 2-aminoethanol (AE). Broken lines in PIES show deconvoluted bands.

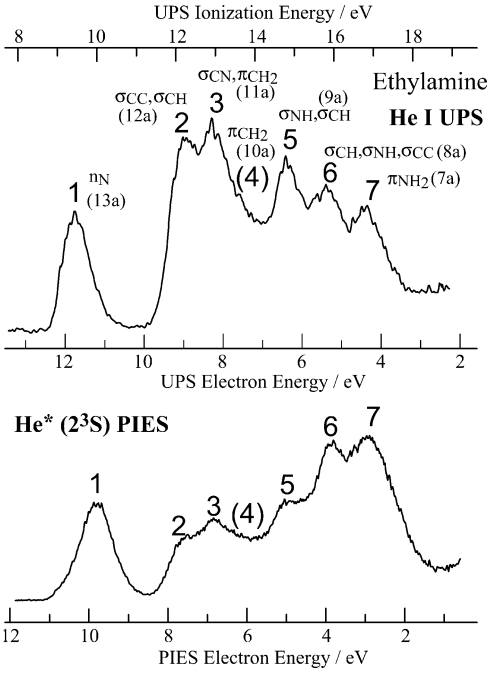

Figure 2. He I UPS and He*(2^3S) PIES of ethylamine (EA).

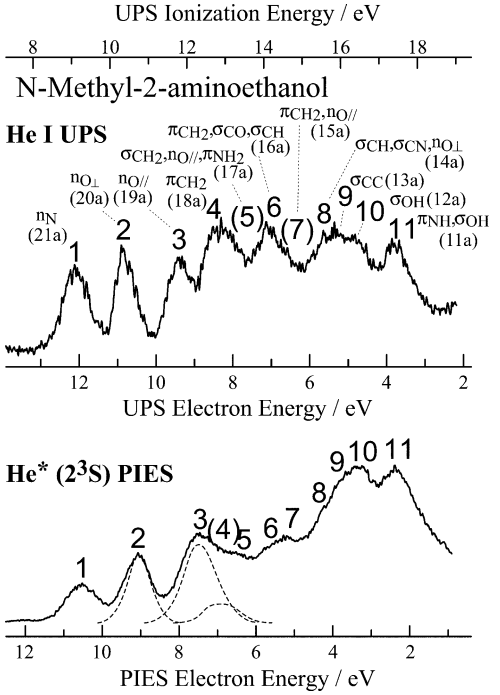

Figure 3. He I UPS and He*(2^3S) PIES of *N*-methyl-2-aminoethanol (MAE). Broken lines in PIES show deconvoluted bands.

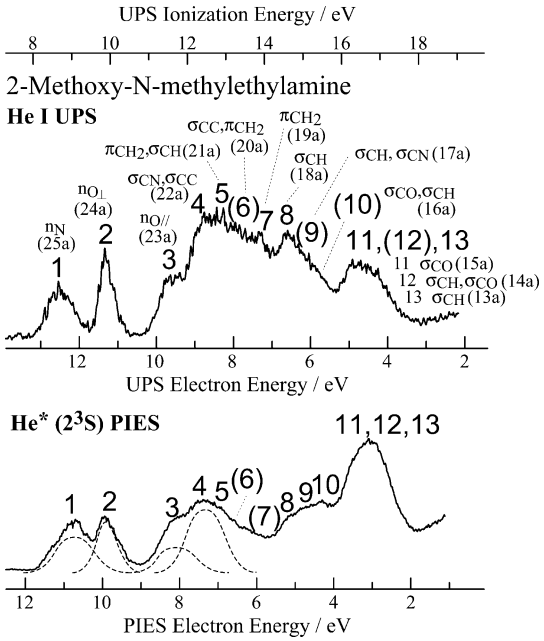

Figure 4. He I UPS and He*(2^3S) PIES of 2-methoxy-*N*-methylethylamine (MMA). Broken lines in PIES show deconvoluted bands.

OH···N hydrogen bond. As shown below, this structure is most preferable to observed characteristics in the present study, although another structure with an NH···O hydrogen bond is slightly more stable (ca. 20 meV) than a structure with an OH···N hydrogen bond. In Tables 2−4, most stable conformers associated with the inversion of the amino group, a gauche conformer for EA and trans conformers for MAE and MMA, were selected according to the calculated MP2 energies. The peak energy shift (ΔE) in PIES measured with respect to the "nominal" energy E_0 (E_0 = the difference between the metastable excitation energy and target ionization potential) is also shown in the tables. Values of the slope m for the log σ vs log E_c plots estimated in a collision energy range of 80−290 meV are also listed in Tables 1−4. Experimental error in each slope parameter m of CEDPICS was estimated to be within ±0.05.

Figures 9−12 show calculated interaction potential energy curves V for AE, EA, and MMA with a ground-state Li (2^2S) atom. Figure 9 shows interaction potential curves $V(R)$ including deepest points of the potential well as a function of the distance R between the Li atom and the N atom in the amino group. Figure 10 shows interaction potential curves $V(\theta)$ as a function of the angle LiNC (θ) for AE as well as EA with keeping the distance R between the Li and N atoms fixed at the minima in Figure 9. To discuss effects of intramolecular bonding in AE, potential energy curves $V(\theta)$ were further studied for the dihedral angle LiNCC (φ) in addition to the angle LiNC (θ), and the

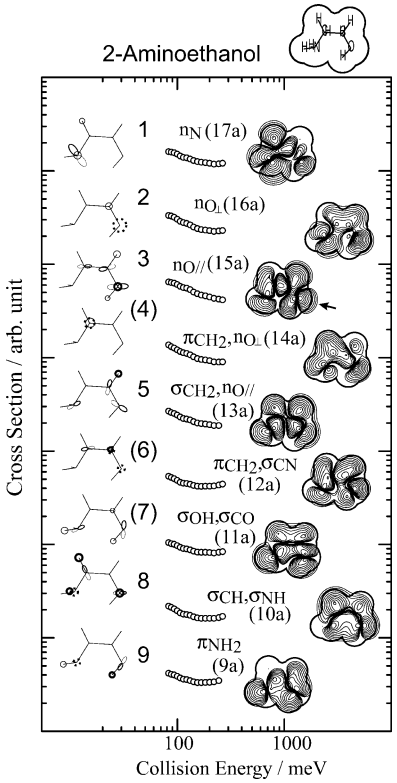

Figure 5. Collision energy dependence of partial ionization cross sections for 2-aminoethanol (AE) with He*(2^3S) atom. The electron density maps and schematic diagram are shown for respective molecular orbitals.

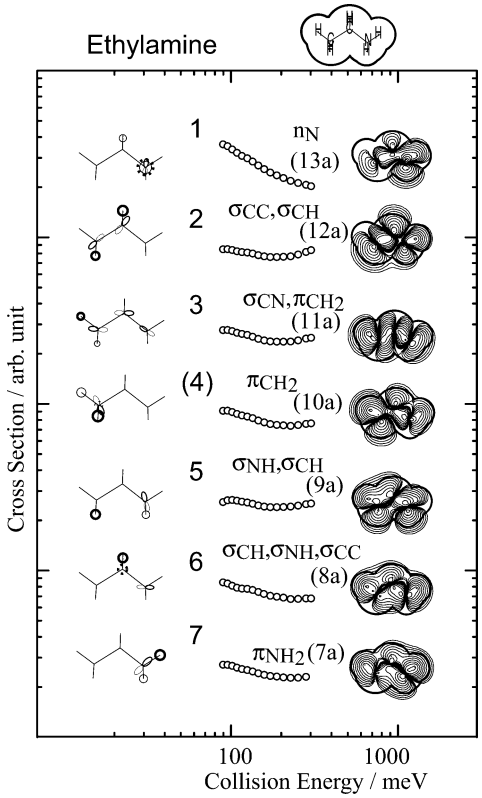

Figure 6. Collision energy dependence of partial ionization cross sections for ethylamine (EA) with He*(2^3S) atom. The electron density maps and schematic diagram are shown for respective molecular orbitals.

results were shown in Figure 11. Figure 12 shows interaction potential curves $V(R)$ including deepest points of the potential well as a function of the distance R between the Li atom and the O atom in the hydroxyl group of AE for a couple of directions; one is in the OCC plane and the other is out of the OCC plane.

V. Discussion

Band Assignments. UPS band assignments of AE and EA have been reported in previous studies,[32,33,36] and these assignments were found to be consistent with the present results in Tables 1 and 2. On the other hand, no UPS data have been reported for MAE and MMA. UPS bands of these molecules were, therefore, assigned by comparing observed UPS and PIES data with those of EA and AE and also with calculated IP values.

Bands 1−3 of MAE were assigned to nonbonding orbitals, n_N, $n_{O\perp}$, and $n_{O\parallel}$ orbitals respectively. Among these bands, the IP values for n_O orbitals were found to be not much different from those for AE, whereas for the n_N orbital, the IP values decreased from 9.75 to 9.21 eV by methyl substitution on the amino group. This tendency can also be seen in calculated IP values for these molecules. It is easy to relate the band 11 at 17.44 eV in the UPS of MAE with the band 9 at 17.61 eV in the UPS of AE. Thus, bands 4−11 as well as bands 1−3 for MAE could be assigned as shown in Table 3. These assignments were found to be consistent with calculated IP values for the trans conformer which is more stable than the gauche conformer by 7 meV.

Bands 1−3 of MMA were assigned to nonbonding orbitals, n_N, $n_{O\perp}$, and $n_{O\parallel}$ orbitals as in the cases of AE and MAE. Since the highest IP band in UPS is also expected around ca. 17 eV, bands 4−13 of MMA were assigned as shown in Table 4.

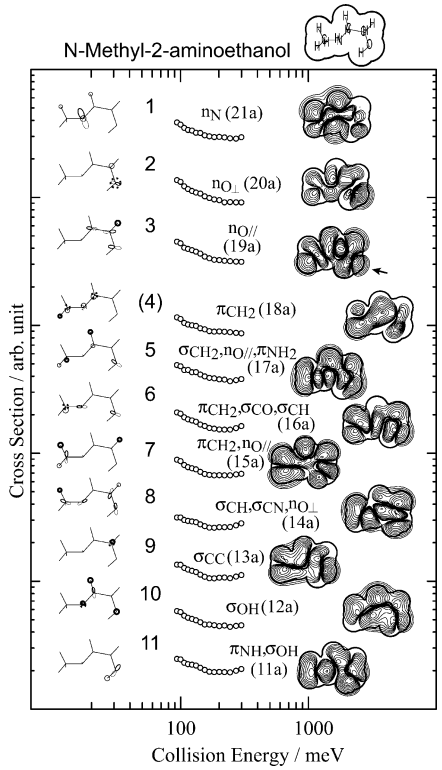

Figure 7. Collision energy dependence of partial ionization cross sections for *N*-methyl-2-aminoethanol (MAE) with He*(2^3S) atom. The electron density maps and schematic diagram are shown for respective molecular orbitals.

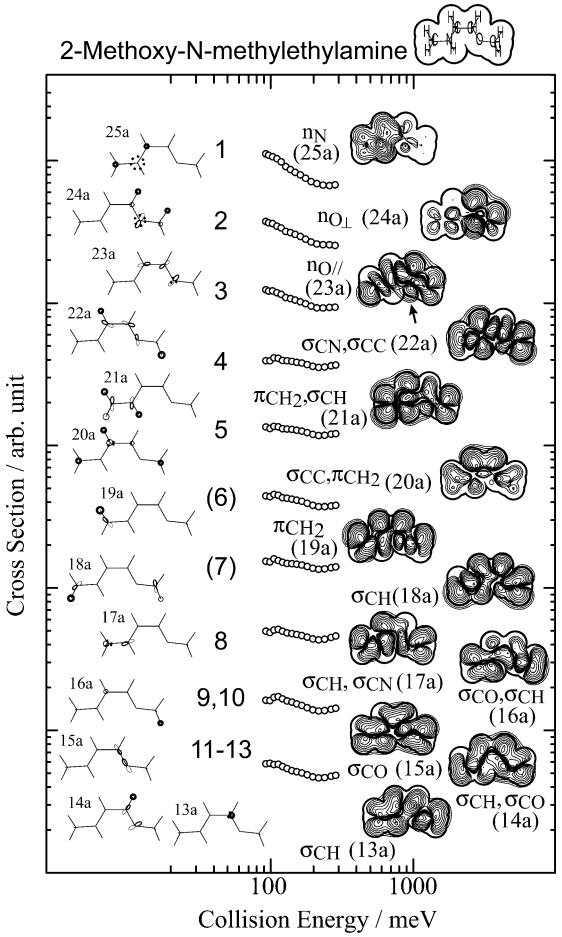

Figure 8. Collision energy dependence of partial ionization cross sections for 2-methoxy-*N*-methylethylamine (MMA) with He*(2^3S) atom. The electron density maps and schematic diagram are shown for respective molecular orbitals.

TABLE 1: Band Assignments, Ionization Potentials (IP_{obsd} and IP_{calcd}/eV), Peak Energy Shifts (ΔE/meV), and Slope Parameters (m) for 2-Aminoethanol (AE, $NH_2CH_2CH_2OH$)

band	IP_{obsd}/eV	IP_{calcd}/eV	orbital character		ΔE/meV	m
1	9.75	11.05	n_N	17a	-350 ± 100	-0.29
2	10.59	11.93	$n_{O\perp}$	16a	-260 ± 30	-0.37
3	11.90	13.24	$n_{O\parallel}$	15a	-500 ± 30	-0.42
4	13.09	14.44	π_{CH_2}, $n_{O\perp}$	14a		(-0.38)
5	14.06	15.38	σ_{CH}, n_O	13a	-200 ± 30	-0.32
6	15.54	16.91	π_{CH_2}, σ_{CN}	12a	-150 ± 60	(-0.19)
7	15.99	17.61	σ_{OH}, σ_{CO}	11a	(-200 ± 30)	(-0.22)
8	16.68	17.93	σ_{CH}, σ_{NH}	10a	-50 ± 30	-0.25
9	17.61	19.32	π_{NH_2}	9a	-100 ± 30	-0.17

Concerning with the observed band positions in UPS, IP values of nonbonding type orbitals has the following orderings among the studied molecules:

IP(n_N): MMA $\sim$ MAE $<$ AE $\leq$ EA

IP(n_O): MMA $<$ MAE $\leq$ AE $<$ (ethanol)[14(c),36]

These orderings show that methyl substitution gives smaller IP values for nonbonding orbitals of substituted nitrogen and oxygen atoms. PIES bands were also assigned in the same ordering as UPS, although some bands related to nonbonding orbitals gave considerably large negative peak shifts of 200−600 meV.

PIES Intensities and Steric Effects. Relative PIES band intensities for nonbonding orbitals, $I(n_N)$, $I(n_{O\perp})$, and $I(n_O)$ were found to be clearly different among AE (Figure 1), MAE (Figure 3), and MMA (Figure 4). Deconvoluted relative intensities for these bands were listed in Table 5. The band intensities for the nitrogen nonbonding orbital $I(n_N)$ in AE and MAE are considerably smaller than that in MMA. This behavior is related to the formation of intramolecular hydrogen bonding of an OH···N type in AE and MAE, which considerably decreases ionization probabilities of the nonbonding orbital of the N atom. This is a shielding effect due to the H atom in the hydrogen bond on the accessibility of other species such as He* atoms onto the electron distributions of the nitrogen nonbonding orbital. Similar effects were reported for a comparison between 2-aminoethanol ($NH_2CH_2CH_2OH$) and 2-methoxyethylamine ($NH_2CH_2CH_2OCH_3$).[33] The $I(n_N)$ value of MAE was found to be smaller than that of AE. This can be ascribed to further reduction of accessibilities of He* atoms onto the electron distributions of the nitrogen nonbonding orbital by the presence of a nearby methyl group, which causes substantial steric shielding effects. Associated with intramolecular hydrogen bonding, interesting steric effects were

TABLE 2: Band Assignments, Ionization Potentials (IP_{obsd} and IP_{calcd}/EV), Peak Energy Shifts (ΔE/meV), and Slope Parameters (m) for Ethylamine (EA, $NH_2CH_2CH_3$, Gauche Form)

band	IP_{obsd}/eV	IP_{calcd}/eV	orbital character		ΔE/meV	m
1	10.06	10.73	n_N	13a	-600 ± 30	-0.51
2	12.31	13.38	σ_{CC}, σ_{CH}	12a	-100 ± 80	-0.07
3	12.97	13.81	σ_{CN}, π_{CH_2}	11a	-30 ± 30	-0.14
4	(13.67)	14.15	π_{CH_2}	10a		(-0.20)
5	14.78	15.85	σ_{NH}, σ_{CH}	9a	0 ± 30	-0.07
6	15.88	17.27	σ_{CH}, σ_{NH}, σ_{CC}	8a	-30 ± 30	-0.21
7	16.86	18.00	π_{NH_2}	7a	-30 ± 30	-0.17

TABLE 3: Band Assignments, Ionization Potentials (IP_{obsd} and IP_{calcd}/EV), Peak Energy Shifts (ΔE/meV), and Slope Parameters (m) for *N*-Methyl-2-aminoethanol (MAE, $NH(CH_3)CH_2CH_2OH$, trans Form)

band	IP_{obsd}/eV	IP_{calcd}/eV	orbital character		ΔE/meV	m
1	9.21	10.39	n_N	21a	-100 ± 30	-0.28
2	10.38	11.86	$n_{O\perp}$	20a	-400 ± 30	-0.41
3	11.80	13.03	$n_{O\parallel}$	19a	-500 ± 30	-0.36
4	12.70	14.29	π_{CH_2}	18a		(-0.22)
5	(13.37)	14.49	σ_{CC}, n_O, π_{NH_2}	17a	-150 ± 30	-0.24
6	14.07	15.51	π_{CH_2}, σ_{CO}, σ_{CH}	16a		-0.27
7	(14.49)	15.74	σ_{CH}, n_O	15a		-0.23
8	15.31	16.99	σ_{CN}, σ_{CH}, $n_{O\perp}$	14a	-30 ± 50	-0.12
9	15.64	17.45	σ_{CC}	13a	-160 ± 50	-0.15
10	16.32	18.18	σ_{OH}	12a	-50 ± 50	-0.26
11	17.44	18.98	π_{NH}, σ_{OH}	11a	-100 ± 30	-0.16

TABLE 4: Band Assignments, Ionization Potentials (IP_{obsd} and IP_{calcd}/EV), Peak Energy Shifts (ΔE/meV), and Slope Parameters (m) for 2-Methoxy-*N*-methylethylamine (MMA, $NH(CH_3)CH_2CH_2OCH_3$, trans Form)

band	IP_{obsd}/eV	IP_{calcd}/eV	orbital character		ΔE/meV	m
1	8.67	9.83	n_N	25a	-450 ± 30	-0.60
2	9.87	11.52	$n_{O\perp}$	24a	0	-0.44
3	11.57	12.83	$n_{O\parallel}$	23a	-60 ± 30	-0.35
4	12.32	13.60	σ_{CN}, σ_{CC}	22a	-30 ± 30	-0.21
5	12.93	13.89	π_{CH_2}, σ_{CH}	21a		-0.21
6	(13.33)	14.31	σ_{CC}, π_{CH_2}	20a		(-0.27)
7	13.86	14.91	π_{CH_2}	19a		(-0.17)
8	14.61	16.00	σ_{CH}	18a	-50 ± 30	-0.22
9	(15.15)	16.25	σ_{CH}, σ_{CN}	17a		} -0.22
10	(15.40)	16.98	σ_{CO}, σ_{CH}	16a		
11	16.29	17.85	σ_{CO}	15a		} -0.26
12	(16.60)	18.32	σ_{CH}, σ_{CO}	14a		
13	17.20	18.60	σ_{CH}	13a		

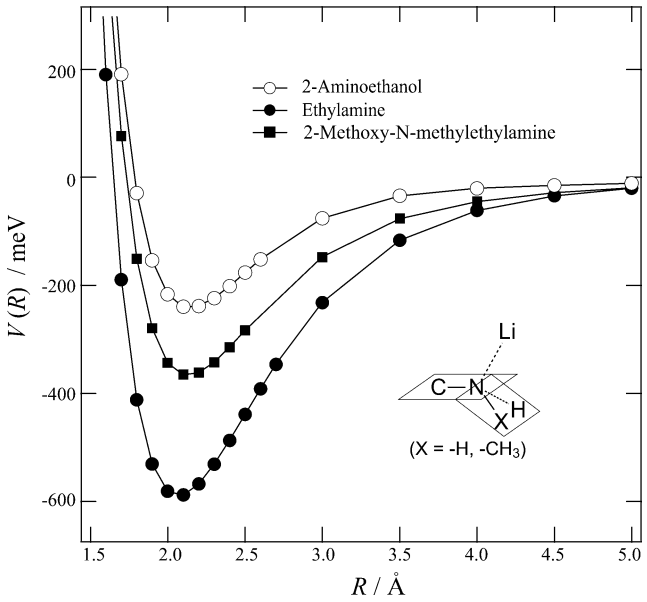

Figure 9. Interaction potential energy curves $V(R)$ as a function of the distance R between Li and N atoms for 2-aminoethanol (○) + Li, ethylamine (●) + Li, and 2-methoxy-*N*-methylethylamine (■) + Li. The Li−N direction taken as follows for 2-aminoethanol ∠LiNC = 141° and the dihedral angle LiNCC = 306°, for ethylamine ∠LiNC = 122° and the dihedral angle LiNCC = 62°, for 2-methoxy-*N*-methylethylamine ∠LiNC = 141°, and the dihedral angle LiNCC = 66°.

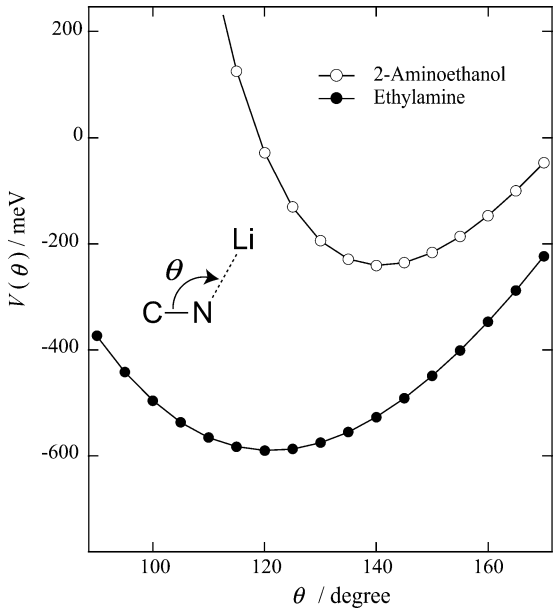

Figure 10. Interaction potential energy curves $V(\theta)$ around the nitrogen atom as a function of angle θ of ∠LiNC. for 2-aminoethanol (○) + Li and ethylamine (●) + Li. The distance R between Li and N atoms is fixed at 2.15 Å for 2-aminoethanol and 2.06 Å for ethylamine.

also found for the band 3 related to ionization from the $n_{O_{||}}$ orbitals. Electron distributions of the $n_{O_{||}}$ orbitals in AE and MAE are extending outside as can be seen in Figures 5 and 7, as indicated by thick solid arrows. On the other hand, the $n_{O_{||}}$ orbital in MMA is only slightly exposed to the outside as indicated by the thick solid arrow in Figure 8. This deactivation of the $n_{O_{||}}$ orbital in MMA is clearly due to formation of intramolecular hydrogen bonding of an NH···O type.

Collision Energy Dependence of Partial Ionization Cross Sections (CEDPICS). Partial ionization cross sections obtained in the present study show mostly negative collision energy

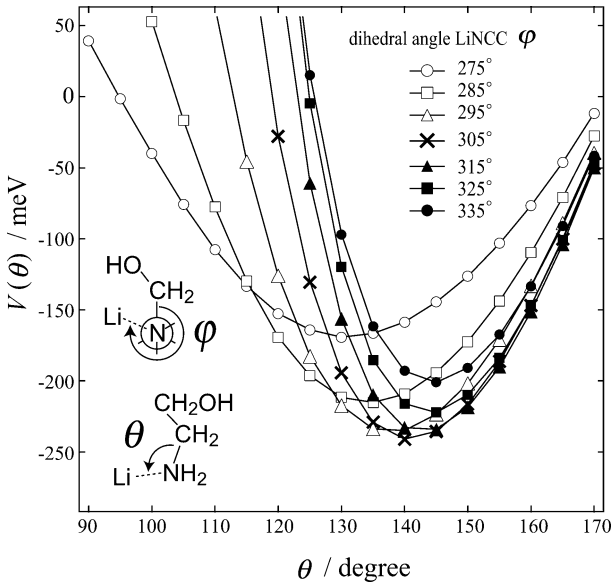

Figure 11. Interaction potential energy curves $V(\theta)$ around the N atom for 2-aminoethanol + Li as a function of angle θ of ∠LiNC. The dihedral angle φ of LiNCC is changed: φ = 275° (○), 285° (□), 295° (△), 305° (×), 315° (▲), 325° (■), and 335.0° (●). The distance R between Li and N atoms is fixed at 2.15 Å for 2-aminoethanol.

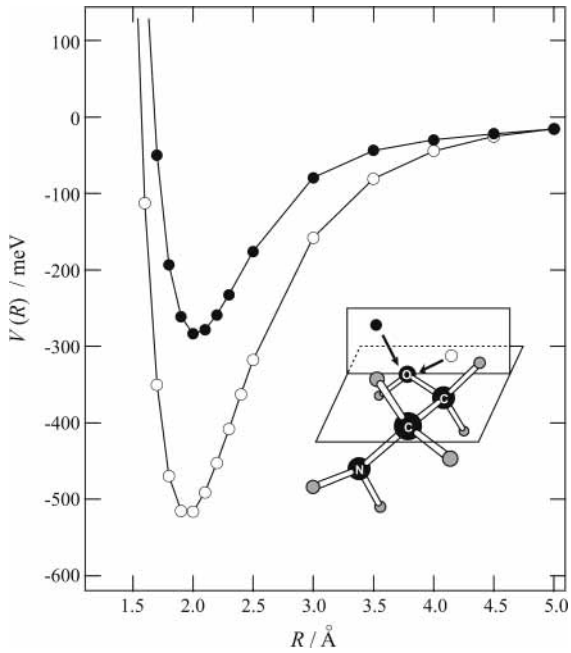

Figure 12. Interaction potential energy curves $V(R)$ for 2-aminoethanol + Li as a function of the distance R. between Li and O atoms along two directions, one in the OCC plane (○) with ∠LiOC = 131°, and the dihedral angle LiOCC = 186° and the other in the vertical plane (●) with ∠LiOC = 125°, and the dihedral angle LiOCC = 90°.

TABLE 5: Relative PIES Intensity of Bands 1−3[a]

molecule	$I(n_N)$ (band 1)	$I(n_{O_\perp})$ (band 2)	$I(n_O)$ (band 3)
$NH_2CH_2CH_2OH$	0.78 ± 0.20	1.00	1.41 ± 0.20
$NH(CH_3)CH_2CH_2OH$	0.61 ± 0.20	1.00	1.18 ± 0.30
$NH(CH_3)CH_2CH_2OCH_3$	1.16 ± 0.30	1.00	0.77 ± 0.20

[a] All intensities are normalized at band 2.

dependence, which is considered to be due to highly attractive interactions around nitrogen and oxygen atoms.[14c,17] Very large negative slopes of $m = -0.60$ and $m = -0.51$ were found for the n_N bands in MMA and EA, respectively. Such a large

negative slope for amines can be related to a deep attractive potential well around the N atom which is free from the hydrogen bonding of an OH···N type. Whereas in the other two systems of AE and MAE, the slope values were found to be much less negative, $m = -0.29$ and $m = -0.28$, respectively. This indicates that attractive interactions around the n_N orbitals are much less effective under the influence of the hydrogen bonding of an OH···N type. Slope values for $n_{O_\perp}$ and $n_{O_\parallel}$ bands were found to be -0.35– -0.44, and thus, interaction potentials around the oxygen atom are highly and widely attractive to He* atoms.

Other regions around CH and NH bonds are considered to be much less attractive or even repulsive from the slope values for bands due to orbitals mainly related to CH and NH bonds. Higher collision energy edges of CEDPICS for band 9 in AE, bands 2 and 5 in EA, and bands 6 and 8 in MAE gave positive collision energy dependence which means that interactions around the hydrogen regions are slightly repulsive.

Peak Energy Shift. According to theoretical considerations by Niehaus,[2,6] peak energy shifts ΔE can be related to approximate potential well depths where ionization transitions take place. Thus, the peak energy shift for the band 1 due to the n_N orbital in each molecule gives an estimate of the potential well depth around the nitrogen atom. Very large ΔE values for the band 1 in EA (-600 ± 30 meV) and MMA (-450 ± 30 meV) correspond to deep potential wells without hydrogen bonding. The small ΔE value for the band 1 in MAE (-100 ± 30 meV) can be ascribed to the influence of intramolecular hydrogen bonding. A little larger ΔE value for the band 1 in AE (-350 ± 100 meV) may be related with spatially much less shielding effects without a neighboring methyl group. Very large negative peak shifts of the band 3 in AE (-500 ± 30 meV) and MAE (-500 ± 30 meV) can be related to deep potential wells in the OCC plane (Figure 12), whereas for negligibly small peak shifts of bands 2 and 3 in MMA indicate that potentials around the oxygen atom are affected by the formation of intramolecular hydrogen bonding of an NH···O type.

Calculated Interaction Potential. As can be seen in Figure 9, calculated depths of attractive potential wells around the N atom of the amino group in MA, MMA, and AE are 590, 360, and 240 meV, respectively. These calculated well depths explain the relative order of the observed negative peak shifts of -600 ± 30 meV in MA, -450 ± 30 meV in MMA, and -350 ± 100 meV in AE. The smallest well depth around the N atom in AE is due to the OH···N type hydrogen bonding. In AE, an intramolecular hydrogen bond of an OH···N type is formed, and the geometrical parameters are as follows: NH(O) length = 2.3 Å, CNH(O) angle = 76.6°, and CCNH(O) dihedral angle = 328.4°. Figure 10 shows that the location of the well minimum in AE is at a higher CNLi angle (θ) of ca. 140°, which is considerably shifted from that (122°) in EA. In AE, the formation of an intramolecular hydrogen bond between H and N atoms prevents the Li atom from the proximity of the H atom in the hydrogen bond, and hence the position of the well minimum becomes at the higher CNLi angle. Steric shielding effects by the H atom in the hydrogen bond are more significant at the higher dihedral LiNCC angle (φ), as can be seen in Figure 11.

Potential energy curves in Figure 12 show depths and directions of the attractive potential well around the O atom in AE. The deep well of -520 meV in the CCO plane corresponds to the observed very large negative peak shift of -500 ± 30 meV for the PIES band 3 ($n_{O_\parallel}$) in AE. The smaller well of -280 meV in a direction vertical to the CCO plane can be ascribed to the observed negative shift of -260 ± 30 meV for PIES band 2 ($n_{O_\perp}$) in AE.

VI. Conclusion

2D-PIES and UPS studies on 2-aminoethanol (AE), ethylamine (EA), *N*-methyl-2-aminoethanol (MAE), and 2-methoxy-*N*-methylethylamine (MMA) revealed interesting spectroscopic aspects associated with intramolecular hydrogen bonding. In AE and MAE, OH···N type hydrogen bonds were found to be preferentially formed, and no apparent supports were obtained for NH···O type hydrogen bonds. On the other hand, in MAE, observed data gave a confirmation of the NH···O type hydrogen bond.

Effects of hydrogen bond formation on several aspects in 2D-PIES were observed for ionization bands of nonbonding orbitals closely related to the hydrogen bond. (1) The relative band intensity in PIES (the partial Penning ionization cross section or the branching ratio) becomes considerably decreased upon hydrogen bond formation, because the accessibility of He* atoms on to the relevant nonbonding orbital is spatially hindered by the presence of the hydrogen bond. (2) The slope of the log−log plot of the collision energy dependence of partial ionization cross section becomes to be much less negative, because attractive potential well regions around the N or O atom are considerably shielded by the H atom in the hydrogen bond. (3) The peak energy shift becomes much less negative, because the presence of the H atom in the hydrogen bond causes the well depths shallower and the accessibility of He* atoms into the well regions lower.

Acknowledgment. This work is partially supported by a Grant in Aid for Scientific Research from the Japanese Ministry of Education, Science and Culture. Authors thank Mr. A. Takada for helpful supports in the experiments. R.M. acknowledges a support from Tohoku University as a Research Assistant.

References and Notes

(1) Penning, F. M. *Naturwissenschaften* **1927**, *15*, 818.
(2) Niehaus, A. *Adv. Chem. Phys.* **1981**, *45*, 399.
(3) Yencha, A. J. In *Electron Spectroscopy: Theory, Techniques and Applications*; Brundle, C. R., Baker A. D., Eds.; Academic Press: New York, 1984; Vol. 5.
(4) Čermák, V. *J. Chem. Phys.* **1966**, *44*, 3781.
(5) Miller, W. H. *J. Chem. Phys.* **1970**, *52*, 3563.
(6) Niehaus, A. *Ber. Bunsen-Ges. Phys. Chem.* **1973**, *77*, 632.
(7) Hotop, H.; Niehaus, A. *Z. Phys. B* **1969**, *228*, 68.
(8) Ohno, K.; Mutoh, H.; Harada, Y. *J. Am. Chem. Soc.* **1983**, *105*, 4555.
(9) Ohno, K.; Matsumoto, S.; Harada, Y. *J. Chem. Phys.* **1984**, *81*, 4447.
(10) Ohno, K.; Yamakado, H.; Ogawa, T.; Yamata, T. *J. Chem. Phys.* **1996**, *105*, 7536.
(11) Ohno, K.; Takami, T.; Mitsuke, K.; Ishida, T. *J. Chem. Phys.* **1991**, *94*, 2675.
(12) Mitsuke, K.; Takami, T.; Ohno, K. *J. Chem. Phys.* **1989**, *91*, 1618.
(13) Kishimoto, N.; Furuhashi, M.; Ohno, K. *J. Electron Spectrosc. Relat. Phenom.* **1998**, *88*−*91*, 143.
(14) (a) Yamakado, H.; Yamauchi, M.; Hoshino, S.; Ohno, K. *J. Phys. Chem.* **1995**, *99*, 17093. (b) Ohno, K.; Okamura, K.; Yamakado, H.; Hoshino, S.; Takami, T. *J. Phys. Chem.* **1995**, *99*, 14247. (c) Kishimoto, N.; Yokoi, R.; Yamakado, H.; Ohno, K. *J. Phys. Chem. A* **1997**, *101*, 3284. (d) Pasinszki, T.; Kishimoto, N.; Ohno, K. *J. Phys. Chem. A* **1999**, *103*, 9195. (e) Kishimoto, N.; Osada, Y.; Ohno, K. *J. Phys. Chem. A* **2000**, *104*, 1393.
(15) Takami, T.; Ohno, K. *J. Chem. Phys.* **1992**, *96*, 6523.
(16) Yamakita, Y.; Yamauchi, M.; Ohno, K. *Chem. Phys. Lett.* **2000**, *322*, 189.
(17) Kishimoto, N.; Furuhashi, M.; Ohno, K. *J. Electron Spectrosc. Relat. Phenom.* **2000**, *113*, 35.

(18) (a) Imura, K.; Kishimoto, N.; Ohno, K. *J. Phys. Chem. A* **2001**, *105*, 4189. (b) Imura, K.; Kishimoto, N.; Ohno, K. *J. Phys. Chem. A* **2001**, *105*, 6073.
(19) Tanaka, H.; Yamakado, H.; Ohno, K. *J. Electron Spectrosc. Relat. Phenom.* **1998**, *88*−*91*, 155.
(20) Radom, L.; Lathan, W. A.; Hehre, W. J.; Pople, J. A. *J. Am. Chem. Soc.* **1973**, *95*, 693.
(21) Gresh, N.; Claverie, P.; Pullman, A. *Theor. Chim. Acta* **1984**, *66*, 1.
(22) Vanquickenborne, L. G.; Coussens, B.; Verlinde, C.; De Ranter, C. *J. Mol. Strct. THEOCHEM.* **1989**, *201*, 1.
(23) Kelterer, A.-M.; Ramek, M. *J. Mol. Struct. THEOCHEM* **1991**, *232*, 189.
(24) Kelterer, A.-M.; Ramek, M.; Frey, R. F.; Cao, M.; Schäfer, L. *J. Mol. Struct. THEOCHEM* **1994**, *310*, 45.
(25) Buemi, G. *Int. J. Quantum Chem.* **1996**, *59*, 227.
(26) Vorobyov, I.; Yappert, M. C.; Dupré, D. B. *J. Phys. Chem. A* **2002**, *106*, 668.
(27) Penn, R. E.; Curl, R. F. *J. Chem. Phys.* **1971**, *55*, 651.
(28) Penn, R. E.; Olsen, R. J. *J. Mol. Spectrosc.* **1976**, *62*, 423.
(29) Tubergen, M. J.; Torok, C. R.; Lavrich, R. J. *J. Chem. Phys.* **2003**, *119*, 8397.
(30) Widicus, S. L.; Drouin, B. J.; Dyl, K. A.; Blake, G. A. *J. Mol. Spectrosc.* **2003**, *217*, 278.
(31) Silva, C. F. P.; Duarte, M. L. T. S.; Fausto, R. *J. Mol. Struct.* **1999**, *482*−*483*, 591.
(32) Leavell, S.; Steichen, J.; Franklin, J. L. *J. Chem. Phys.* **1973**, *59*, 4343.
(33) Ohno, K.; Imai, K.; Harada, Y. *J. Am. Chem. Soc.* **1985**, *107*, 8078.
(34) Takami, T.; Mitsuke, K.; Ohno, K. *J. Chem. Phys.* **1991**, *95*, 918.
(35) Gardner, J. L.; Samson, J. A. R. *J. Electron Spectrosc. Relat. Phenom.* **1976**, *8*, 469.
(36) Kimura, K.; Katsumata, S.; Achiba, Y.; Yamazaki, T.; Iwata, S. *Handbook of He I Photoelectron spectra of fundamental organic molecules*; Japan Scientific: Tokyo, 1981.
(37) Kishimoto, N.; Aizawa, J.; Yamakado, H.; Ohno, K. *J. Phys. Chem. A* **1997**, *101*, 5038.
(38) Caminati, W. *Mol. Phys.* **1987**, *121*, 61.
(39) Becke, A. D. *J. Chem. Phys.* **1993**, *98*, 5648.
(40) Pauling, L. *The Nature of Chemical Bond*; Cornell University Press: Ithaca, New York, 1960.
(41) Rothe, E. W.; Neynaber, R. H.; Trujillo, S. M. *J. Chem. Phys.* **1965**, *42*, 3310.
(42) Illenberger, E.; Niehaus, A. *Z. Phys. B* **1975**, *20*, 33.
(43) Parr, T. P.; Parr, D. M.; Martin, R. M. *J. Chem. Phys.* **1982**, *76*, 316.
(44) Hotop, H. *Radiat. Res.* **1974**, *59*, 379.
(45) Haberland, H.; Lee, Y. T.; Siska, P. E. *Adv. Chem. Phys.* **1981**, *45*, 487.
(46) Frisch, M. J.; Truckss, G. W.; Schlgel, H. B.; Gill, P. M. W.; Johnsin, B. G.; Robb, M. A.; Cheeseman, J. R.; Keith, T.; Petersson, G. A.; Montogomery, J. A.; Raghavachari, K.; Al-Laham, M. A.; Zakrzewski, V. G.; Ortiz, J. V.; Foresman, J. B.; Cioslowski, J.; Stefanov, B. B.; Nanayakkara, A.; Challacombe, M.; Peng, C. Y.; Ayala, P. Y.; Chen, W.; Wong, M. W.; Andres, J. L.; Replogle, E. S.; Gomperts, R.; Martin, R. L.; Fox, D. J.; Binkley, J. S.; Defrees, D. J.; Baker, J.; Stewart, J. P.; Head-Gordon, M.; Gozalez, C.; Popple, J. A. *Gaussian 98*, revision A.11.4; Gaussian Inc.: Pittsburgh, PA, 2002.
(47) Ohno, K.; Takano, S.; Mase, K. *J. Phys. Chem.* **1986**, *90*, 2015.